Supplementary Materials for Multi-satellite constraints reduce uncertainty in modeled aerosol forcing

Yusuf Bhatti[1*], Leighton Regayre[2,3,4], Hailing Jia[1], Duncan Watson-Parris[5], Nick Schutgens[6], Athanasios Nenes[7,8], Ulas Im[9], Bastiaan van Diedenhoven[1], Ardit Arifi[1], Guangliang Fu[1], Xuemei Wang[10], Carl Svenhag[9], Gerd-Jan van Zadelhoff[10], Otto Hasekamp[1]

[1]SRON Space Research Organisation Netherlands, Leiden, Netherlands.
[2]Met Office Hadley Centre, Exeter, UK.
[3]Centre for Environmental Modelling and Computation, University of Leeds, Leeds, UK.
[4]School of Earth and Environment, University of Leeds, Leeds, UK.
[5]Scripps Institution of Oceanography and Halıcıoğlu Data Science Institute, University of California San Diego, La Jolla, CA, USA.
[6]Vrije Universiteit Amsterdam, Amsterdam, Netherlands.
[7]Institute of Chemical Engineering Sciences, FORTH/ICE-HT, Patras, Greece.
[8]School of Architecture, Civil and Environmental Engineering (ENAC), Laboratory of Atmospheric Processes and their Impacts (LAPI), Ecole Polytechnique F'ed'erale de Lausanne (EPFL), Lausanne, Switzerland.
[9]Aarhus University, Department of Environmental Science, Roskilde, Denmark.
[10]Royal Netherlands Meteorological Institute (KNMI), Utrecht, Netherlands.

*Corresponding author(s). E-mail(s): y.bhatti@sron.nl ;

Abstract

This PDF file includes:

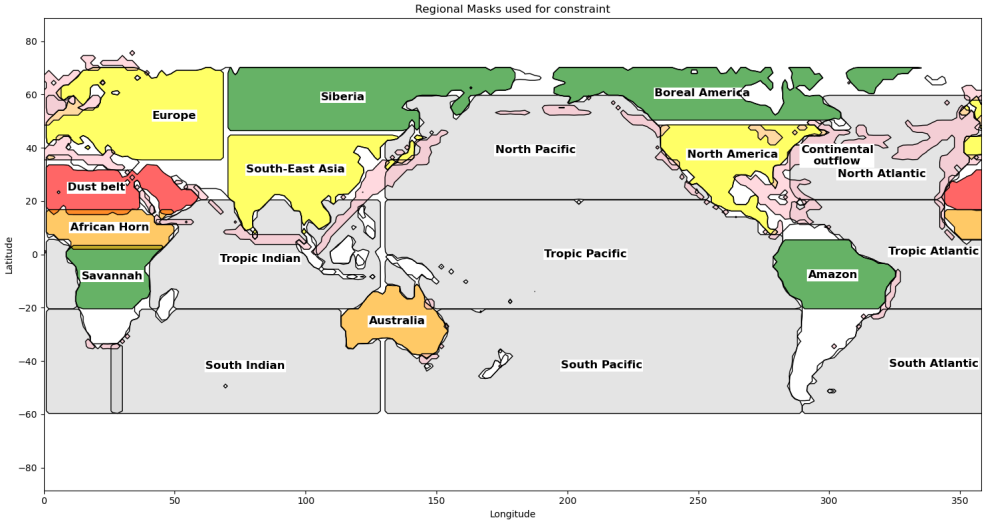
Supplementary Figures 1 to 13

Supplementary Tables 1 to 2

Supplementary Notes 1

Supplementary Table 1 Parameters used in the PPE, grouped by process category, with their prescribed minimum and maximum ranges.

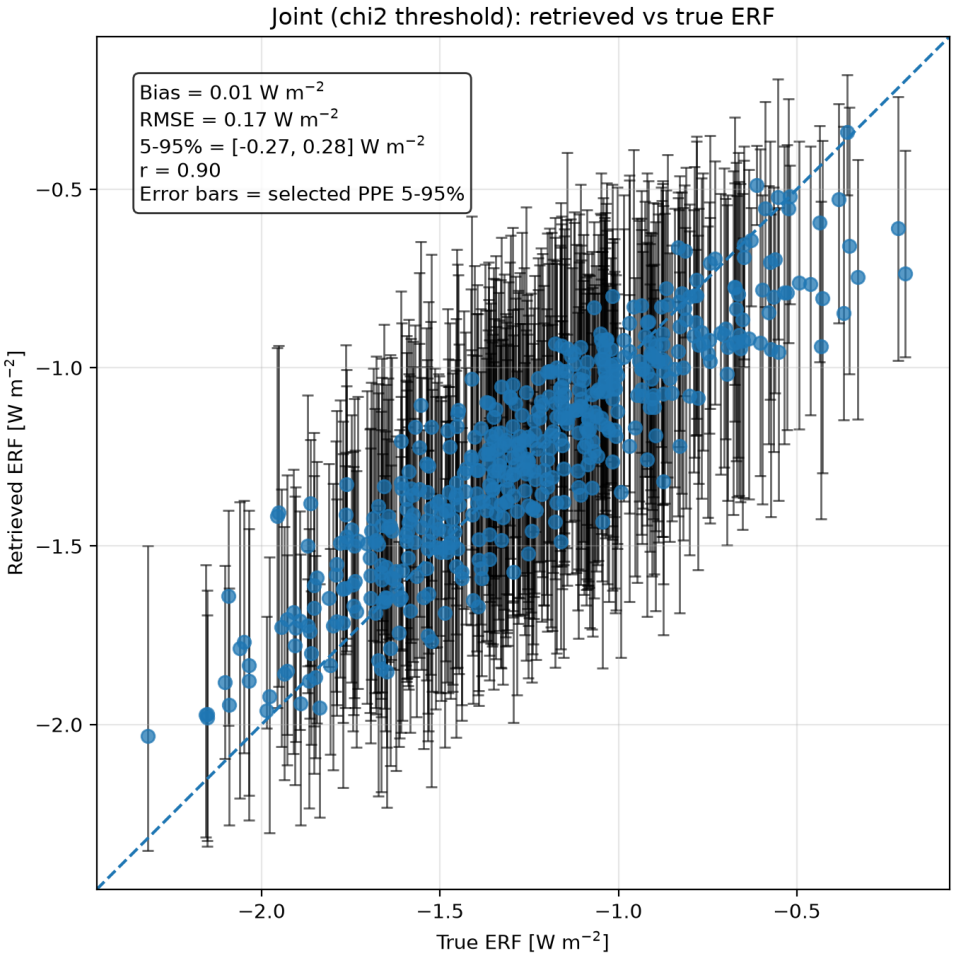
Parameter	Description	Min	Max
Natural emissions			
EMI_DMS	DMS emissions scaling	0.2	3
EMI_SS_ACC	Sea salt emission (accumulation mode)	0.1	3
EMI_SS_COARSE	Sea salt emission (coarse mode)	0.1	3
Anthropogenic emissions			
EMI_SHP_SO2	Ship SO_2 emissions	0.25	5
EMI_ANTNS_SO2	Anthropogenic SO_2 emissions	0.6	2
EMI_ANT_BC	Anthropogenic BC emissions	0.6	2
EMI_ANT_OC	Anthropogenic OC emissions	0.6	2
Biomass burning emissions			
EMI_BB_SO2	Biomass burning SO_2 emissions	0.25	4
EMI_BB_BC	Biomass burning BC emissions	0.25	4
EMI_BB_OC	Biomass burning OC emissions	0.25	4
Aerosol diameter			
EMI_CMR_FF	Fossil fuel emission diameter	1.5×10^{-8}	4.5×10^{-8}
EMI_CMR_BB	Biomass burning emission diameter	2.5×10^{-8}	2.5×10^{-7}
FRICV	Friction velocity of dust scaling	0.845	1.08
SEASALT_EXPO	Sea salt emission parameterisation exponent	0.9	1.1
Optics and absorption			
BC_RAD_NI	BC refractive index	0.2	0.9
DU_RAD_NI	Dust refractive index	2×10^{-4}	1×10^{-2}
OC_RAD_NI	OC refractive index	1×10^{-4}	1×10^{-1}
SO_4COATING	Sulfate coating (aging)	0.3	5
KAPPA_SO4	Sulfate hygroscopicity	0.3	0.8
KAPPA_OC	OC hygroscopicity	0.02	0.4
Chemistry			
SO2_REACTIONS	SO_2 oxidation rates	0.5	2
DMS_REACTIONS	DMS oxidation rates	0.5	2
Removal processes			
WETDEP_IC	In-cloud wet deposition	0.75	1.25
WETDEP_BC	Below cloud wet deposition	0.33	3
DRYDEP_ACC	Dry deposition (accumulation mode)	0.1	10
Cloud microphysics			
ACTIVATION	Aerosol activation	0.75	1.25
VERTICAL_VELOCITY	Updraft velocity scaling	0.5	2
NUC_FT	Free-tropospheric and boundary layer nucleation	0.01	10



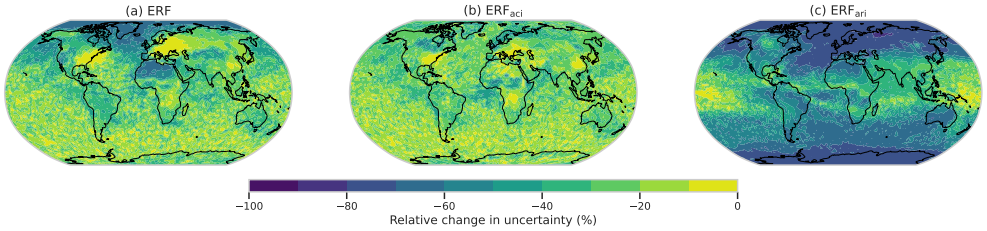
Supplementary Figure 1 Regional masks used to average diagnostics into 19 distinct aerosol and cloud regimes for constraint.

Supplementary Table 2 Satellite observations used for the constraint. Tolerances represent observational uncertainty (Methods). Where two values are given, the larger of the absolute and relative tolerance is used.

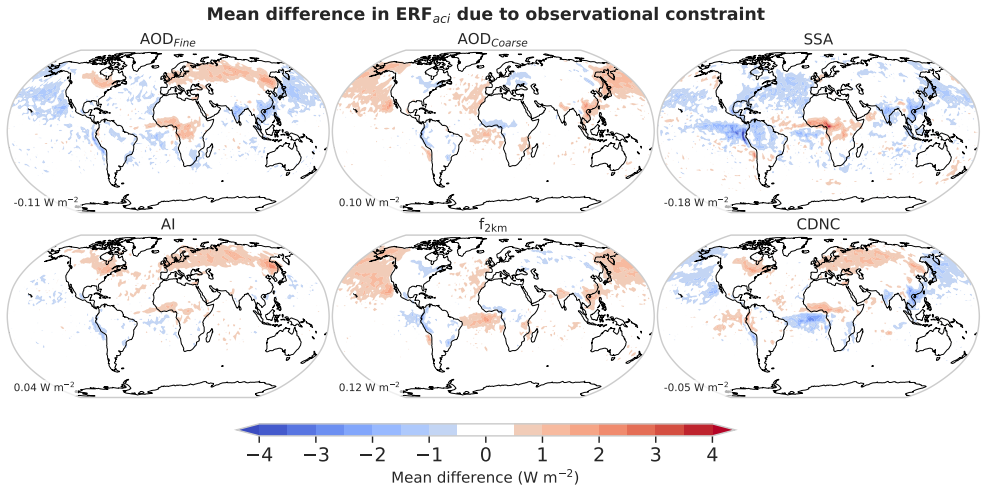
Instrument (satellite)	Variable	Sampling	Tolerance	Symbol
SPEXone (PACE)	Fine-mode aerosol optical depth at 550 nm (Aitken and accumulation modes)	3-hourly	0.02 or 10%	$\mathrm{AOD}_{\mathrm{fine}}$
SPEXone (PACE)	Coarse-mode aerosol optical depth at 550 nm	3-hourly	0.02 or 10%	$\mathrm{AOD}_{\mathrm{coarse}}$
SPEXone (PACE)	Single scattering albedo at 550 nm	3-hourly	0.035	SSA
SPEXone (PACE)	Aerosol index (AOD × Ångström exponent)	3-hourly	0.02 or 10%	AI
OCI (PACE)	Cloud droplet number concentration	Daily	50%	N_d
OCI (PACE)	Hemispheric contrast in cloud droplet number concentration	Daily	50%	$\Delta\mathrm{N}_d$
ATLID (EarthCARE)	Fraction of column aerosol extinction below 2 km	Daily	10%	$f_{2\mathrm{km}}$



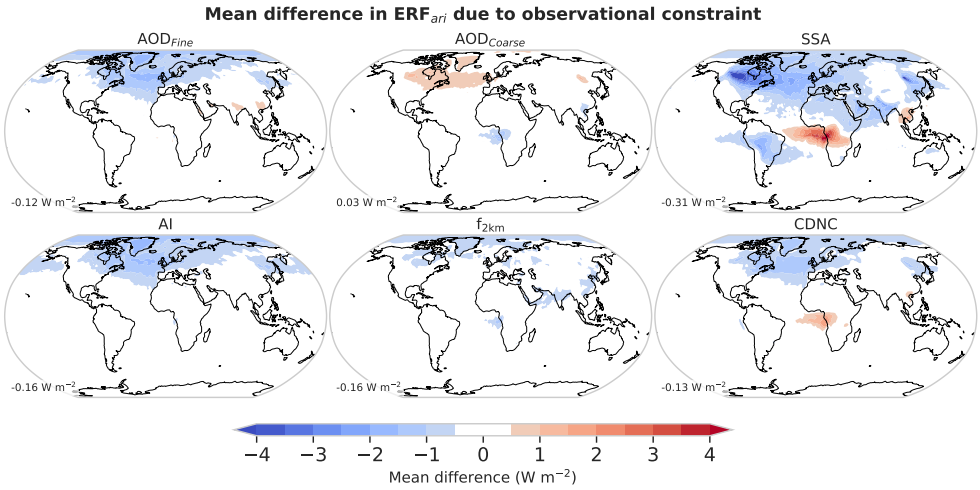
Supplementary Figure 2 Synthetic test of the joint observational constraint. Each dot represents a model variant (out of 500) that is randomly sampled from the emulated PPE and treated as a known truth. The x-axis shows the true global annual-mean effective radiative forcing (ERF) against the (y-axis) ERF retrieved by applying the joint constraint to synthetic observations of all six observables. The synthetic observations include noise with standard deviations equal to the tolerances in Supplementary Table 2. Error bars show the 5-95% range of the accepted variants for each truth, and the dashed line is the 1:1 line. The legend shows the mean bias (retrieved minus true ERF), the root-mean-square error (RMSE), the 5-95% range of the retrieval errors, and the correlation coefficient (r) across the 500 truths.



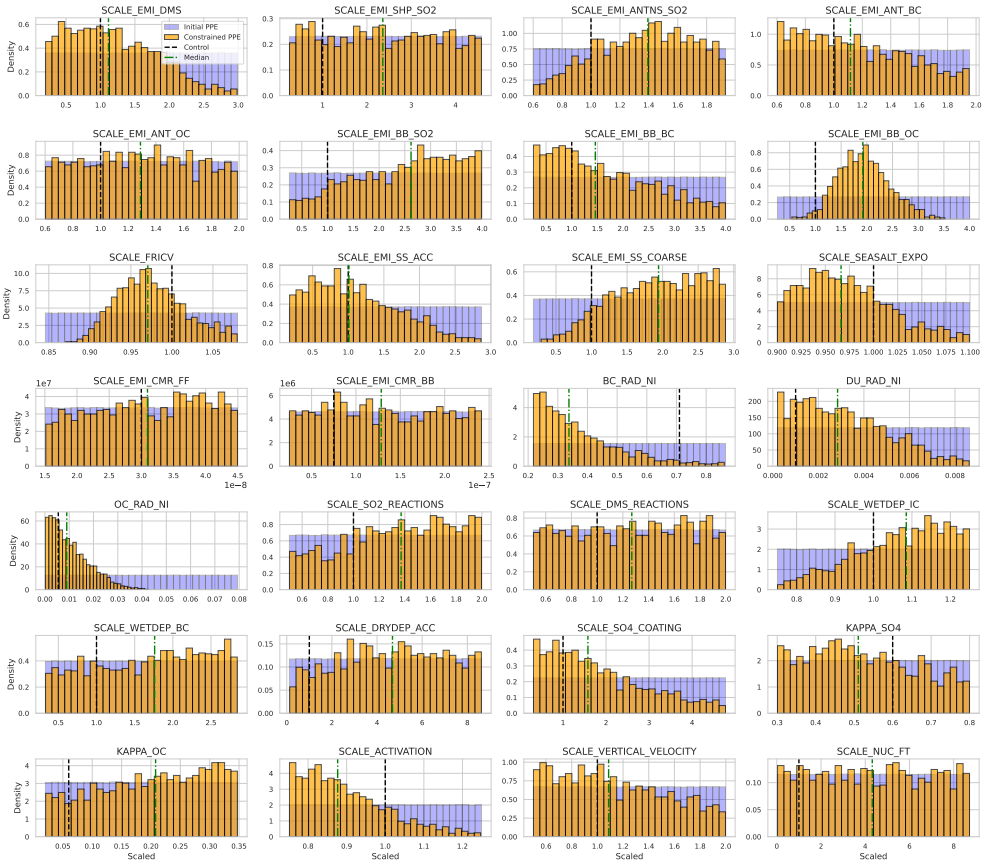
Supplementary Figure 3 Similar to Figure 2, but showing the relative uncertainty reduction of ERF, ERF$_{aci}$, and ERF$_{ari}$. The relative change is calculated at each grid cell as $100 \times (\sigma_c - \sigma_u)/\sigma_u$, where σ_u is the standard deviation of the unconstrained ensemble (2 million emulated samples) and σ_c that of the constrained ensemble (1290 accepted samples). A value of -100% indicates that the uncertainty is fully removed, with 0% indicating no change.



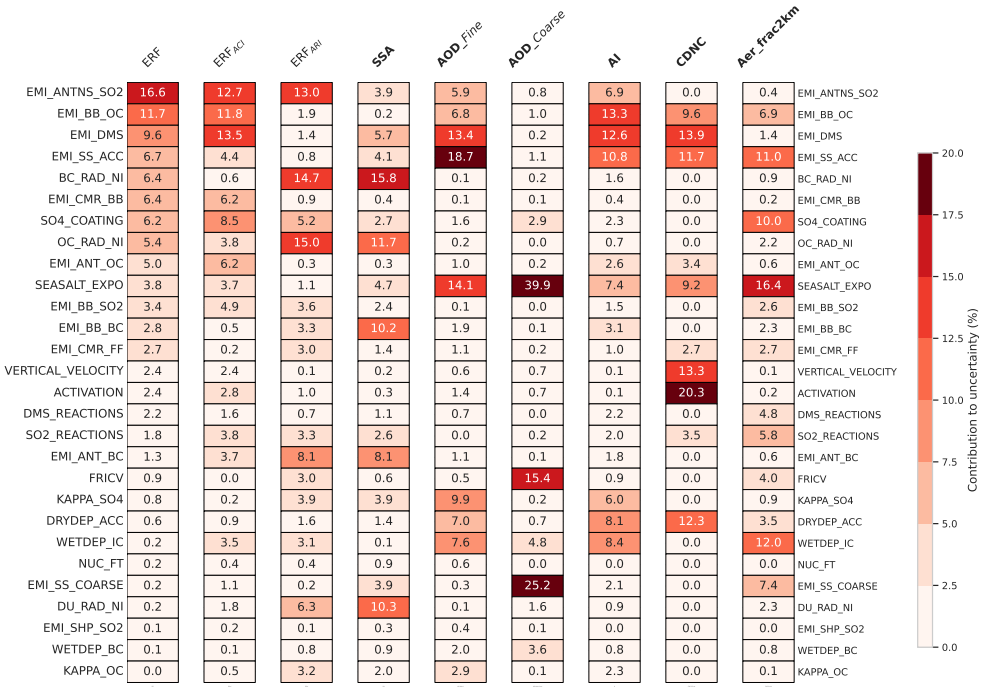
Supplementary Figure 4 Same as Fig. 4 in the main text, but showing ERF$_{aci}$.



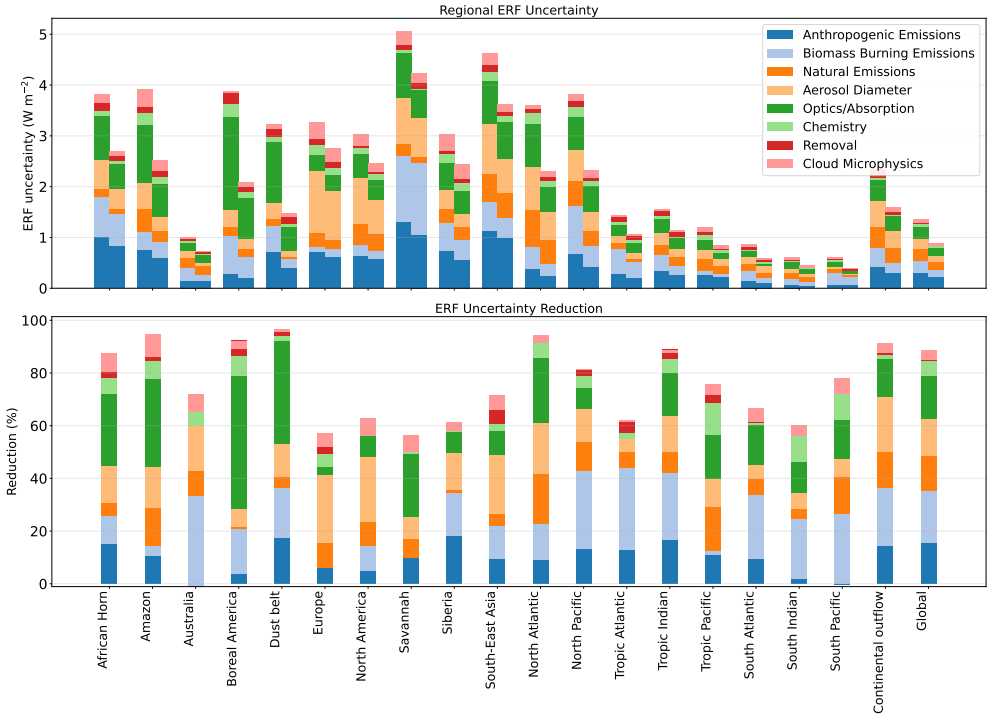
Supplementary Figure 5 Same as Fig. 4 in the main text, but showing ERF$_{ari}$.



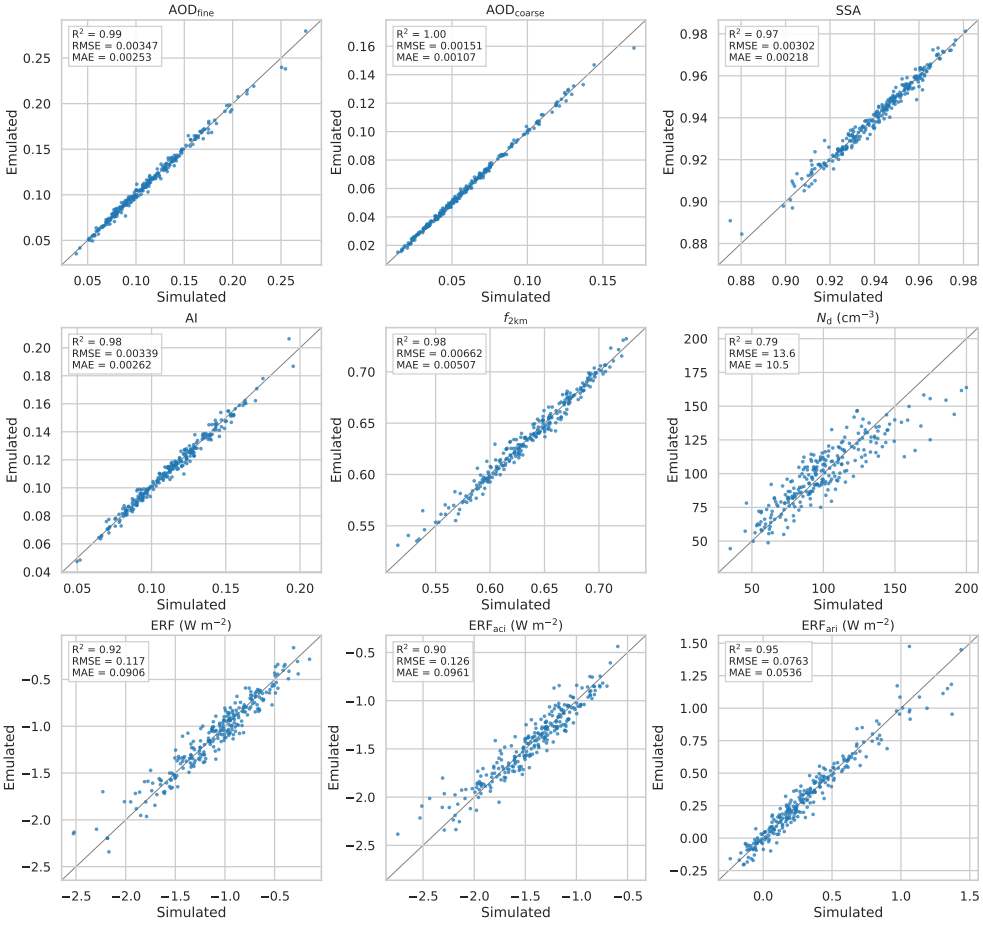
Supplementary Figure 6 Prior and posterior parameter distributions for the PPE under the joint observational constraint. Histograms show the initial PPE (prior; blue) and the constrained PPE (posterior; orange) for each perturbed parameter (titles). Vertical lines indicate the control value and the ensemble medians (as shown in the legend). Parameters include emissions scalings (e.g., DMS, anthropogenic and biomass-burning species, sea-salt), aerosol optical parameters (e.g., refractive index scalings), chemical production terms, removal processes, hygroscopicity (kappa), and activation-related parameters.



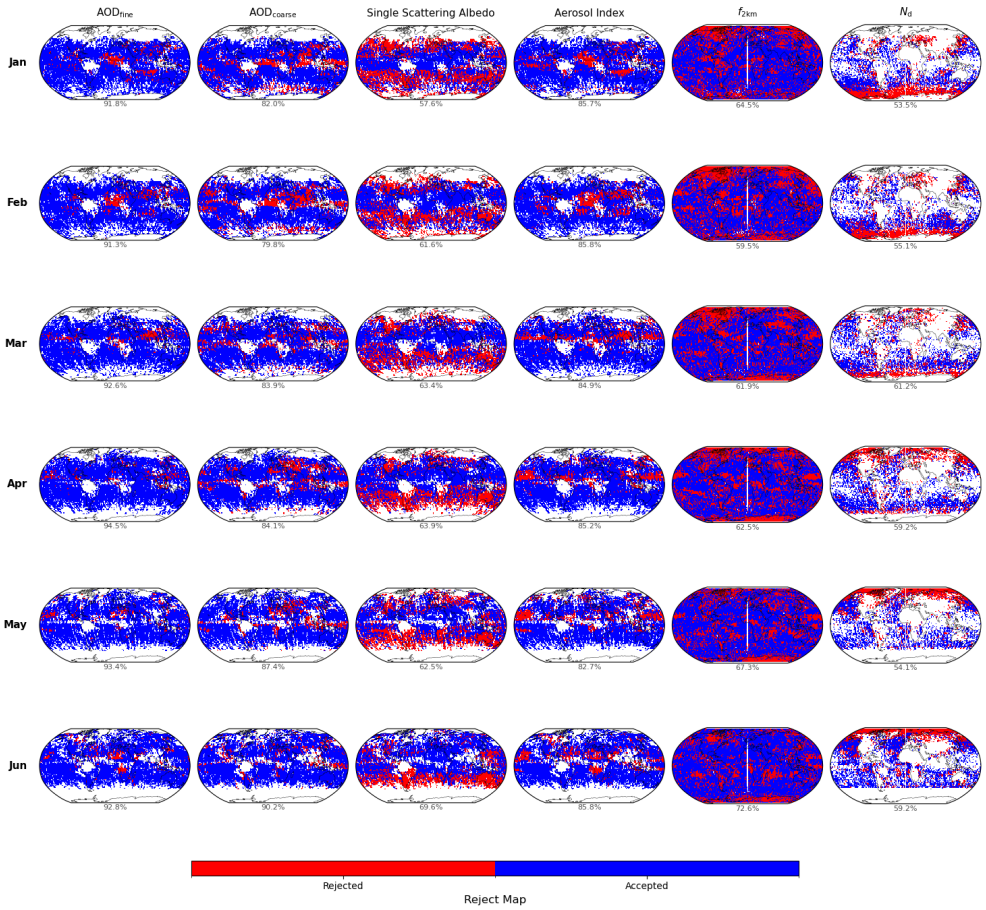
Supplementary Figure 7 Variance-based sensitivity from the emulator. This is shown as the contribution of individual model parameters to global annual mean uncertainty (5-95% range) in ERF and satellite-observable diagnostics. Each cell shows the percentage of total uncertainty in a given diagnostic (columns) attributable to each parameter (rows), with parameters ordered by their contribution to total ERF uncertainty (left column). Diagnostics include total ERF, ERF_{aci}, ERF_{ari}, single scattering albedo (SSA), fine-mode AOD, coarse-mode AOD, aerosol index (AI), cloud droplet number concentration (N_d), and aerosol fraction below 2 km.



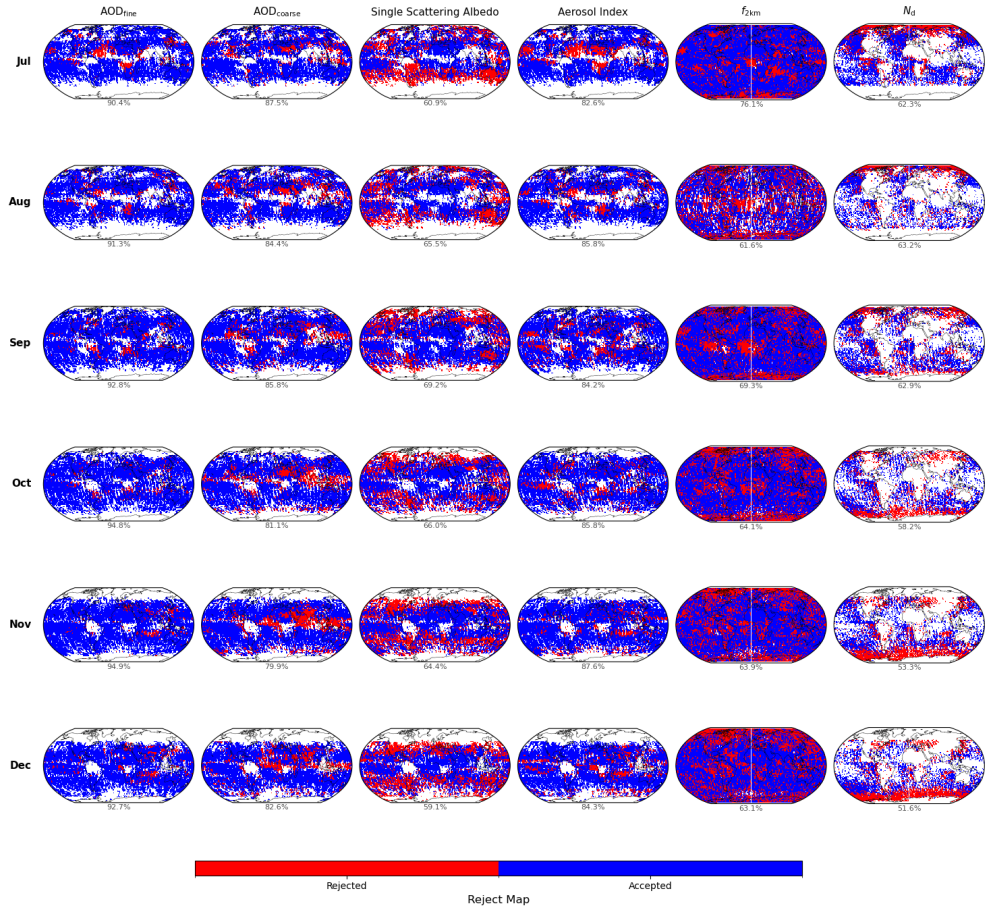
Supplementary Figure 8 Regional ERF uncertainty by parameter group, before and after observational constraint. (*Top*) Total ERF uncertainty (5-95% range, W m^{-2}) for each region prior to constraint (left bar) and remaining after applying the combined satellite observational constraint (right bar).(*Bottom*) Percentage reduction in ERF uncertainty achieved by the combined constraint, by parameter group. Colours show different parameter groups: anthropogenic emissions (dark blue), biomass burning emissions (light blue), natural emissions (dark orange), aerosol diameter (light orange), optics/absorption (dark green), chemistry (light green), removal (red), and cloud microphysics (pink)



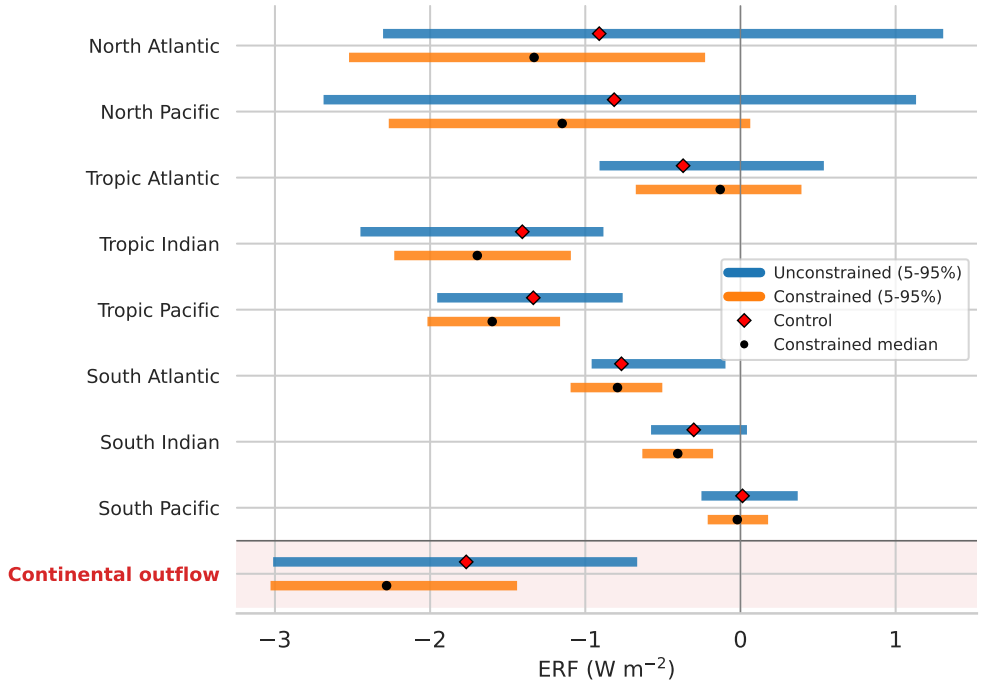
Supplementary Figure 9 Emulator validation for (a) $\mathrm{AOD_{fine}}$, (b) $\mathrm{AOD_{coarse}}$, (c) SSA, (d) AI, (e) $f_{2\mathrm{km}}$, (f) N_d, (g) ERF, (h) ERF_{aci} and (i) ERF_{ari}. Each dot is the global annual mean of one PPE member from ECHAM6-HAM (x-axis) against the predicted PPE member from the emulator (y-axis). The gray line indicates a perfect relationship. The coefficient of determination (R^2), root-mean-square error (RMSE), and mean absolute error (MAE) are shown for each diagnostic.



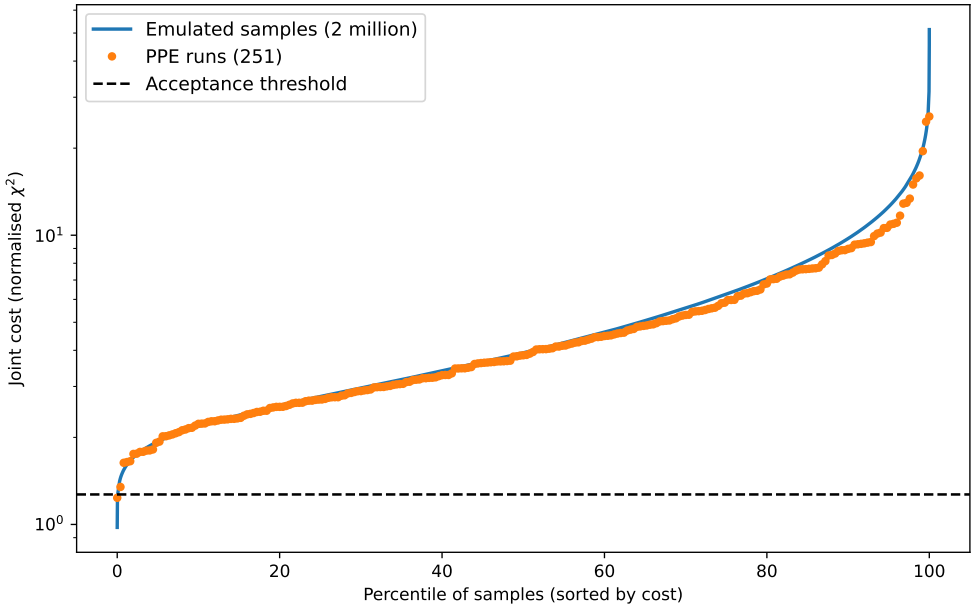
Supplementary Figure 10 Monthly rejection masks used to exclude locations where model-observation mismatch is dominated by structural error or representativeness limitations before constraint. Columns show the six diagnostics used for the masking step ($\mathrm{AOD_{fine}}$, AOD_{Coarse}, SSA, AI, $\mathrm{f_{2km}}$, and N_d). Rows show individual months over the analysis period (January to June). Blue grid cells indicate locations retained for constraint, and red grid cells indicate rejected locations; maps are masked to the spatial coverage of each observational product. Percentages denote the fraction of grid cells retained for that diagnostic in each month.



Supplementary Figure 11 Same as Fig. 10 but showing July to December.



Supplementary Figure 12 Regional aerosol effective radiative forcing over the ocean regions. Blue bars show the 5th to 95th percentile range of the unconstrained ensemble and orange bars show the constrained ensemble. Red diamonds represent the control simulation and black dots the median of the constrained ensemble. The continental outflow region (shaded) is calculated (Figure 1) where CEDS ship SO_2 emissions exceed five times the mean ship SO_2 emission over the ocean.



Supplementary Figure 13 Joint cost (normalized χ^2) of the 2 million emulated samples (blue) and the 251 simulated PPE members (orange), sorted by cost and plotted against their percentile. The dashed line shows the acceptance threshold, below which 1290 emulated samples out of 2 million.

Supplementary Note 1: Effective radiative forcing calculation

In ECHAM6-HAM, each radiation call is performed twice per timestep: once with the full aerosol distribution (all-sky, *with* aerosols) and once with aerosol radiative effects suppressed (the "no-aerosol" call, as na), enabling clean separation of aerosol-radiation and aerosol-cloud effects.

The total ERF is defined as the change in net top-of-atmosphere (TOA) all-sky radiative flux (F) between the present-day (PD) and pre-industrial (PI) simulations:

$$\mathrm{ERF} = F^{\mathrm{PD}}_{\mathrm{TOA}} - F^{\mathrm{PI}}_{\mathrm{TOA}}, \tag{S1}$$

call diagnostic, as the difference between the all-sky and no-aerosol, F_{na}, fluxes:
The ERF due to aerosol-radiation interactions ($\mathrm{ERF}_{\mathrm{ari}}$) is calculated using the double-

$$\mathrm{ERF}_{\mathrm{ari}} = \left(F^{\mathrm{PD}} - F^{\mathrm{PD}}_{\mathrm{na}}\right) - \left(F^{\mathrm{PI}} - F^{\mathrm{PI}}_{\mathrm{na}}\right), \tag{S2}$$

The ERF due to aerosol-cloud interactions ($\mathrm{ERF}_{\mathrm{aci}}$) is calculated by:

$$\mathrm{ERF}_{\mathrm{aci}} = \left(F^{\mathrm{PD}}_{\mathrm{na}} - F^{\mathrm{PD}}_{\mathrm{cs,na}}\right) - \left(F^{\mathrm{PI}}_{\mathrm{na}} - F^{\mathrm{PI}}_{\mathrm{cs,na}}\right), \tag{S3}$$

where $\mathrm{cs,na}$ is clear-sky, no-aerosol fluxes. As a result, $\mathrm{ERF} \approx \mathrm{ERF}_{\mathrm{ari}} + \mathrm{ERF}_{\mathrm{aci}}$, with any residual attributable to surface albedo and other minor terms [1].

References

[1] Ghan, S. J. Technical Note: Estimating aerosol effects on cloud radiative forcing. *Atmospheric Chemistry and Physics* **13**, 9971–9974 (2013). URL https://acp.copernicus.org/articles/13/9971/2013/.